

Ultra-high LRS Nonlinearity and high speed in HfO_x Based Complementary Resistive Switch with Ti electrode for Vertical RRAM

Yu-Sheng Chen, Pang-Shiu Chen¹, Heng-Yuan Lee, Kan-Hsueh Tsai, Tai-Yuan Wu, Fred Chen, and Ming-Jinn Tsai

Electronics and Optoelectronics Research Laboratory, Industrial Technology Research Institute, Hsinchu 310, Taiwan. ¹Department of Chemical and Materials Engineering, MingShin University of Science & Technology Hsinfong, Hsinchu 304, Taiwan, Phone : 886-3-5593142 ext 3377, Fax : 886-3-5593142, E-mail : pschen@must.edu.tw

Abstract A reactive Ti of 5 nm thick can improve the memory window of HfO_x device with complementary resistive switch (CRS). The CRS HfO_x device exhibits high LRS nonlinearity (>1000), robust retention at 150 °C, and enough endurance (>1000) at 40 ns speed. A plausible mechanism is proposed.

1. Introduction

Due to high speed, low power, and 3D stack feasibility, random access resistive memory (RRAM) shows a promising potential for being the next generation high density nonvolatile memory [1,2]. To solve the cost issue for RRAM applied in high storage field, vertical RRAM (VRRAM) structure is proposed to substantially reduce the critical mask number [2]. Besides the tight process margin for fabrication of one selector-one resistor (1S1R) device in VRRAM, as reading out the high resistance state (HRS) of the memory cell, the sneak current flows through the device in low resistance state (LRS) by a middle electrode (ME) between the selector and RRAM, and by ME and top electrode (TE). Complementary resistive switch (CRS) cells are promising devices, which can be integrated in VRRAM to solve this issue [3]. However, both devices suffer poor LRS nonlinearity and their high temperature retention is less addressed. In this work, the HfO_x based CRS with ultra-high LRS nonlinearity is demonstrated. Possible filament models are proposed.

2. Device Fabrication and measurement

The TiN/HfO_x/TiN (NHN), TiN/Ti/HfO_x/TiN (THN) and TiN/Ti/HfO_x/Ti/TiN (THT) devices with 10, 15 and 20 nm HfO_x layers as shown in Fig. 1. The inserted Ti layer of 5 or 10 nm-thick were prepared. The HfO_x film and metal electrodes were deposited by ALD and sputtering. All devices with 0.36 μm cell size were annealed at 450 °C. The microstructure of the device was investigated by XTEM. XPS was used to analyze the composition depth profile. The *I-V* were characterized by using HP 4156A. 50 devices were measured to examine their electrical uniformity. The endurance of the CRS were studied by the stress mode of HP 4156A combined with the pulse mode of 81110A.

3. Results and Discussion

The device needs an initial forming step before the bistable resistive switching. After forming, there are two kinds of operation mode. Case I, the device under negative voltage sweeping can operated with a typical BRS mode. Case II, the NHN devices are operated along the positive voltage sweep with or without compliance current (*I*_{comp}) as shown in Fig. 2. (The sequential without *I*_{comp} is referred as the 2nd forming step). Without *I*_{comp}, the resistance of the device increase abruptly. The plausible mechanism of the HfO_x base device during 2nd forming step with or without *I*_{comp} is proposed in Fig. 3. The models of hourglass shape filaments composed of O vacancies for LRS are proposed, the migration of ions under the ramped voltage lead to the resistance transition [3]. The NH(15)N device exhibits the coexistence of the BRS and CRS (Fig. 5), depending on whether the 2nd forming step is used [3,4]. In Fig. 6, the XTEM image of T(5)H(15)T(5) device is present, the inserted one is the compositional profile of T(5)H(15)T(5) stacked layer revealed by XPS analysis. The Ti capping layer and buffer layer can getter excessive O ions from the HfO_x layer. The BRS of the T(5)H(15)T(5) device is also evaluated. Fig. 7. The typical forming and 1st RESET *I-V* curves for the TH(15)T device with BRS mode, however, the RESET step can not be successful. But,

the TH(15)T device is formed with 2nd forming step, a resistance transition in the device occur ~ 1.0 V. The ratio of the resistance transition in the THT device is larger than that of NHN one. Effect of asymmetric electrode configuration of THN and THT devices under the 2nd forming step and followed by a negative voltage sweeping are shown in Fig. 8. Inserting 5 nm Ti layers in the interfaces between HfO_x and TiN significantly improves the CRS characteristic under the 40 ns speed (Fig. 9). However, the 10 nm Ti layers obviously degrade the CRS performances of HfO_x device. The typical *R-V* curves for the NHN, T(5)HT(5), T(10)HT(10) devices under the 2nd forming step with the pulse width of 40 ns are depicted in Fig. 9. With a 5 nm Ti inserted layer, the device exhibits a large resistance transition during the 2nd forming. Fig. 10 shows the ultra-high LRS nonlinearity, defined as $R_{\pm 0.5V}/R_{\pm 1.5V}$, above 1000 in the T(5)H(15)T(5) device. The Weibull plot of $R_{\pm 0.5V}$ and $R_{\pm 1.5V}$ distributions for the NHN, T(5)HT(5), T(10)HT(10) devices under positive and negative sweep with pulse widths of 40 ns are shown in Fig. 11. The stable operation voltages are also demonstrated in this device with tight resistance distributions (Fig. 12). According to the compositional analyses in inserted of Fig. 6, the thickness of the TiO_x layers due to captured O ions by Ti layers from HfO_x film increases as the thicker Ti layers are inserted. Thus, besides the conventional hourglass shape filament model [5,6], the Ti layers effect on filaments structures needs to be considered. The thin TiO_x layers, being enough O ions reservoirs, enhance the completeness of filaments rupture at both polarities and improve the HRS magnitude. For the device with thicker Ti layers, due to more O vacancies in HfO_x, the stronger filaments near interfaces are formed. Lower HRS values are attributed to the defective recovery oxide in the HfO_x film after RESET, which may result in a low resistance transition in T(10)HT(10) device.

The typical *R-V* curves for the T(5)H(15)T(5) device under the 2nd forming step with the pulse width of 40 ns and 1 ms are shown in Fig. 13. Long operation time can supply excessive energy to form strong filaments in the device at the end of the 2nd forming (Fig. 14), the results suggest that the CRS device can operated with high speed. The T(5)H(15)T(5) device exhibits good thermal stability of CRS operation at 150 °C for 500 min (Fig. 15). No resistance degradation is observed. The CRS endurance with good nonlinearity exceeds than 1000 cycles with the pulse width of 40 ns by using ramped-up voltage method under the 100 kΩ HRS criterion (Fig. 16). The On/Off ratio is ~ 120.

4. Conclusions

A simple stacked layer of HfO_x with BRS or CRS mode with different forming process is demonstrated. Two steps of forming process can trig NHN device with CRS mode. A reactive Ti can improve the memory window of HfO_x with CRS mode. The CRS HfO_x device with 5 nm Ti layers exhibits high LRS nonlinearity (>1000), robust retention at 150 °C, and enough endurance (>1000) at 40 ns speed. The filament structure may be responsible for the thickness effect of Ti on the performance of HfO_x with CRS property. The CRS devices still suffer high operation current; some new approaches are used to reduce the operation current.

5. References

- [1] H. Y. Lee *et al.*, IEDM, p. 460, 2010. [2] S. G. Park *et al.*, IEDM, p. 501, 2012. [3] F. Nardi *et al.*, IEDM, p. 709, 2011. [4] H. Y. Lee *et al.*, VLSI-TSA, 2013, p. 36. [5] C. B. Lee, *APL*, vol. 93, p. 042115, 2008. [6] F. Nardi *et al.*, *IEEE TED*, vol. 60, p. 70, 2012.

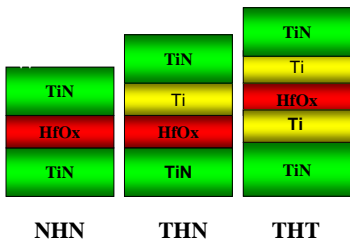


Fig. 1. Schematic diagrams of NHN, THN, and THT stacked layer in this work.

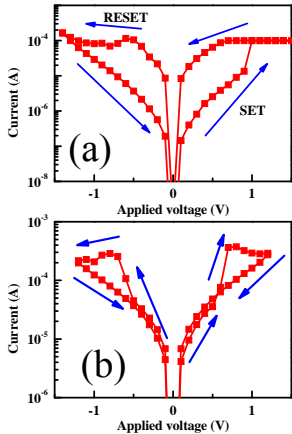


Fig. 5. Coexistence of (a) BRS and (b) CRS in the NH(10)N device with double voltage sweeping operation.

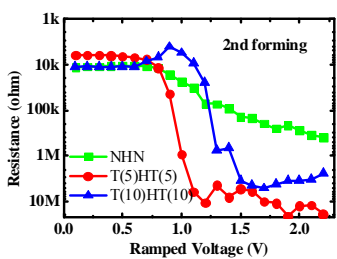


Fig. 9. The typical R - V curves for the NHN, T(5)HT(5), T(10)HT(10) devices under the 2nd forming step with the pulse width of 40 ns.

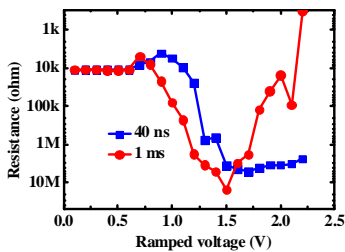


Fig. 13. The typical R - V curves for the T(5)H(15)T(5) device under the 2nd forming step with the pulse width of 40 ns and 1 ms.

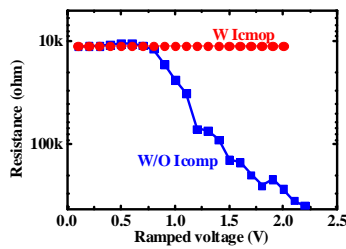


Fig. 2. The typical R - V curves of NHN device with or without a I_{comp} during the 2nd forming step along the positive voltage sweep.

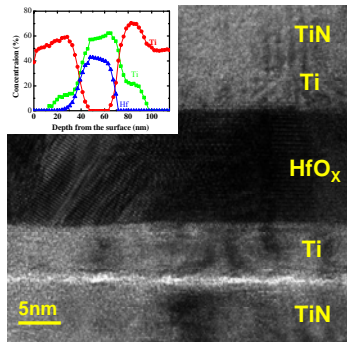


Fig. 6. XTEM image of T(5)HT(5) device, the inserted one is the compositional profile of T(5)HT(5) revealed by XPS analysis.

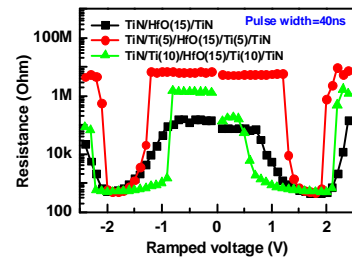


Fig. 10. Typical R - V curves of NHN, T(5)HT(5), T(10)HT(10) devices under positive and negative sweep with pulse widths of 40 ns.

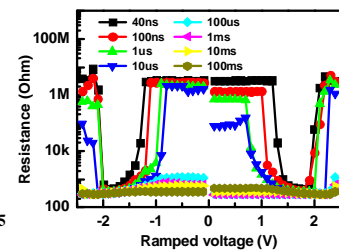


Fig. 14. Typical R - V curves of Ti(5)H(15)Ti(5) device under positive and negative sweep with different pulse widths.

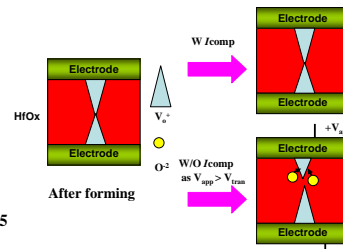


Fig. 3. The plausible mechanism of the HfO_x base device during 2nd forming step with or without I_{comp} .

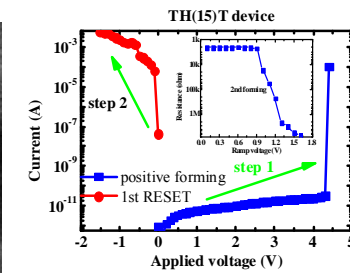


Fig. 7. The typical forming and 1st RESET I - V curves for the TH(15)T device with BRS mode, the TH(15)T device were formed with 2nd forming step, the current in the device was not clamped during the 2nd forming process.

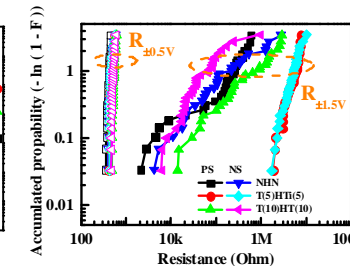


Fig. 11. The Weibull plot of $R_{0.5V}$ and $R_{41.5V}$ distributions for the NHN, T(5)HT(5), T(10)HT(10) devices under positive sweep and negative with pulse widths of 40 ns.

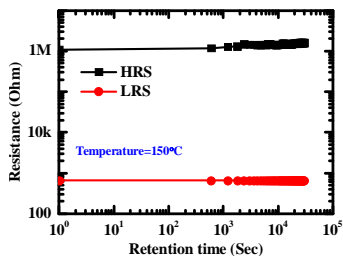


Fig. 15. Data Retention of T(5)H(15)T(5) CRS device at 150 °C. The device shows a robust memory maintenance performance.

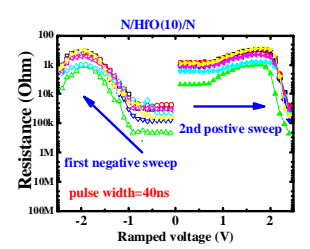


Fig. 4. The typical R - V curves of the NHN device under the first NS and the following PS. The NHN devices show CRS characteristics.

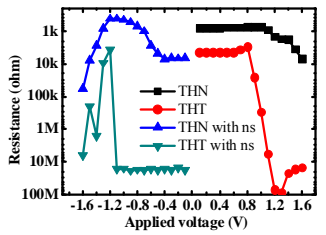


Fig. 8. Effect of asymmetric electrode configuration of THN and THT devices under the 2nd forming step and followed by a negative voltage sweeping.

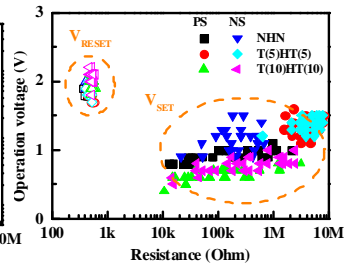


Fig. 12. Dependence of operation voltages on the resistance for the LHS and HRS of the NHN, T(5)HT(5), T(10)HT(10) devices under positive sweep and negative with pulse widths of 40 ns.

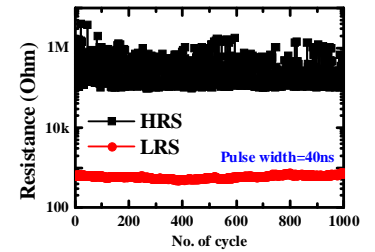


Fig. 16. CRS endurance of T(5)H(15)T(5) CRS device operated by ramped-up voltage

Acknowledgement This work is supported by the National Science Council through Grant No. NSC 101-2221-E-159-019-.